UCRL-TR-220687

LAWRENCE
LIVERMORE
NATIONAL
LABORATORY

Comparison of the LLNL ALE3D and AKTS Thermal Safety Computer Codes for Calculating Times to Explosion in ODTX and STEX Thermal Cookoff Experiments

A. P. Wemhoff
A. K. Burnham

April 19, 2006

This work was performed under the auspices of the U. S. Department of Energy by the University of California, Lawrence Livermore National Laboratory, under Contract No. W-7405-Eng-48.

DISCLAIMER

Abstract

Cross-comparison of the results of two computer codes for the same problem provides a mutual validation of their computational methods. This cross-validation exercise was performed for LLNL's ALE3D code and AKTS's Thermal Safety code, using the thermal ignition of HMX in two standard LLNL cookoff experiments: the One-Dimensional Time to Explosion (ODTX) test and the Scaled Thermal Explosion (STEX) test. The chemical kinetics model used in both codes was the extended Prout-Tompkins model, a relatively new addition to ALE3D. This model was applied using ALE3D's new pseudospecies feature. In addition, an advanced isoconversional kinetic approach was used in the AKTS code. The mathematical constants in the Prout-Tompkins code were calibrated using DSC data from hermetically sealed vessels and the LLNL optimization code Kinetics05. The isoconversional kinetic parameters were optimized using the AKTS Thermokinetics code. We found that the Prout-Tompkins model calculations agree fairly well between the two codes, and the isoconversional kinetic model gives very similar results as the Prout-Tompkins model. We also found that an autocatalytic approach in the beta-delta phase transition model does affect the times to explosion for some conditions, especially STEX-like simulations at ramp rates above 100 °C/hr, and further exploration of that effect is warranted.

Table of Contents

Introduction

The time, as a function of external temperature, for thermal ignition of a finite body of exothermic reacting materials is of broad interest for industrial and military applications. The case of most interest to LLNL is the thermal ignition of a high explosive. Thermal ignition occurs when the material self-heats to a temperature at which the rate of energy generation exceeds the rate of energy dissipation by thermal conduction, and the material undergoes rapid heating. Since the rate of heat generation has an Arrhenius dependence ($k = A\exp(-E/RT)$), where A is a frequency factor and E is an activation energy, the rate rises very sharply with temperature near the ignition time.

ALE3D, which stands for Arbitrary Lagrangian-Eulerian in Three Dimensions, is used in many LLNL applications to predict both the timing and violence of thermal ignition events (e.g., Yoh et al., 2005). It is also used in numerous other applications and by many other governmental organizations. ALE3D includes the calculation of chemical reactions, thermal transport, and material movement and deformation. Most previous applications of ALE3D have used chemical reactions that exhibit an Arrhenius temperature dependence and that depend on the concentration of one or more materials to the n^{th}-power, where n is an integer. Recently, an autocatalytic model adapted from Prout and Tompkins (Burnham, 2000) was installed into ALE3D, since explosives tend to have autocatalytic mechanisms.

AKTS Thermal Safety is a 1D code that is used around the world to predict the timing of thermal ignition events for both military and industrial applications (Roduit, 2004). It is a much simpler code that excludes material movement or deformation, but it does allow for temperature-dependent thermal properties. It can model spheres, infinite cylinders, and infinite slabs. Its primary chemical reaction approach is an advanced isoconversional method, which uses 100 A-E pairs sequentially for each percent of reaction. This program is set up to read these parameters from the output file of the AKTS Thermokinetics program (Roduit, 2004), which uses regression methods to calibrate the A-E pairs against experimental data having a uniform temperature over the sample for a set of arbitrary thermal histories. A similar regression capability exists in the LLNL code Kinetics05 (Burnham and Braun, 1999; Burnham et al., 2004). The AKTS Thermal Safety program also has the option of a user-input model, such as the Prout-Tompkins model, that is a nonlinear regression option in Kinetics05. A feature just added to the AKTS Thermal Safety code allows input of isoconversional parameters derived by other programs as well.

Having this set of codes, it is desirable to perform thermal ignition calculations using the same parameters in ALE3D and AKTS Thermal Safety. Correspondence of results provides mutual validation. In addition, a comparison to results using the isoconversional approach in AKTS Thermal Safety program provides a partial assessment of the desirability of that approach. The isoconversional approach generally can provide a better fit to complex reaction profiles with less user direction, so it is potentially a type of model that should be installed in ALE3D in the future.

Optimization of Kinetic Parameters

The experimental results used to calibrate the chemical kinetic model have been described in detail elsewhere (Burnham and Weese, 2004). Basically, 0.5 mg or less of HMX was heated in a sealed aluminum pan at rates of 0.1, 0.35, and 1.0 ^{o}C/min in a Differential Scanning Calorimeter (DSC). The time-temperature-reaction rate data was supplied to both the AKTS Thermokinetics and LLNL Kinetics05 programs. Both programs optimized the isoconversional kinetic model, and Kinetics05 optimized the extended Prout-Tompkins model:

$$-\frac{dx}{dt} = -kx^n(1-qx)^m \tag{1}$$

where n is a reaction order, m is a nucleation-growth parameter, and q is an initiation parameter (usually 0.99). The fitted parameters are:

$A = 3.81\times10^{13}$ s^{-1}
$E = 39297$ kcal/mol
$n = 0.320$
$m = 0.635$.

The isoconversional model used in Kinetics05 is based on Friedman's method (Friedman, 1964), in which A and E factors are determined at 1% reaction intervals by linear regression to an Arrhenius relation:

$$\ln\left[\left(\frac{1}{x}\right)\left(-\frac{dx}{dt}\right)\right] = \ln A - \frac{E}{RT} \tag{2}$$

where x is the mass fraction of reactant remaining. The isoconversional method in AKTS Thermokinetics is similar, but more complicated, and the details have not yet been released. Regardless, Figure 1 shows that the two programs give very similar results for the same data set except for the last few percent of reaction, which is dominated by baseline uncertainty and is not important for calculating thermal ignition. Figure 2 compares the fits of the isoconversional and extended Prout-Tompkins model from Kinetics05 to the DSC data. The isoconversional model fits better because of the greater degrees of freedom.

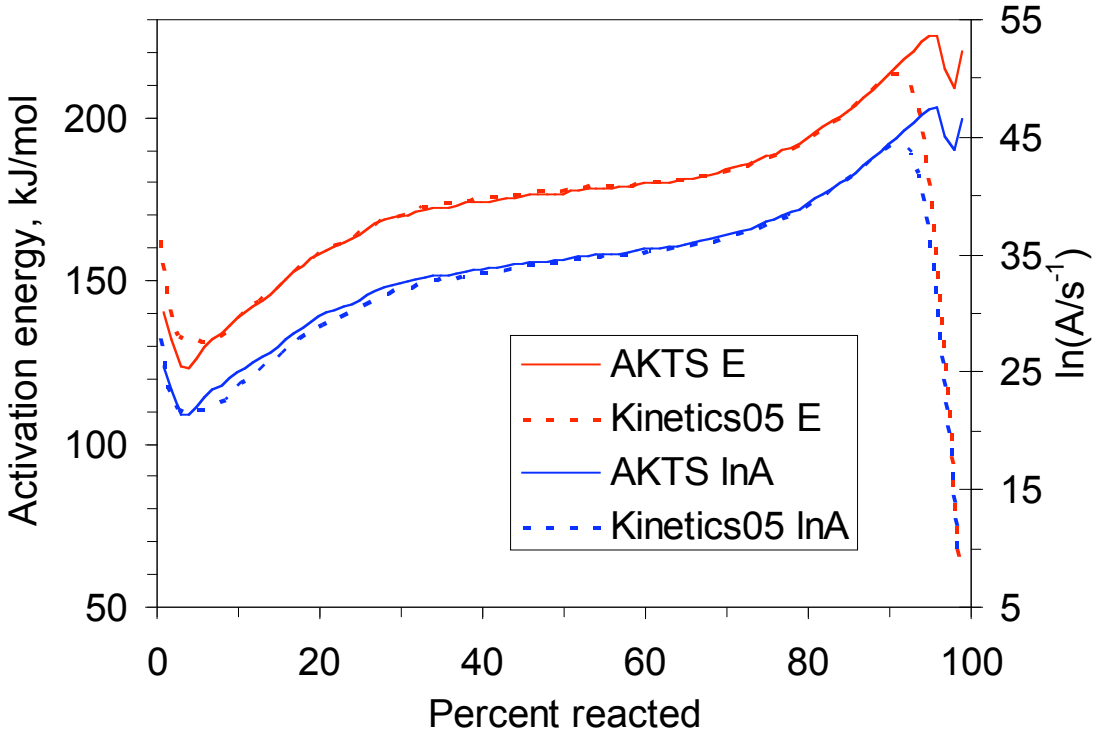

Figure 1. Comparison of HMX isoconversional kinetic parameters from the AKTS Thermokinetics and LLNL Kinetics05 programs.

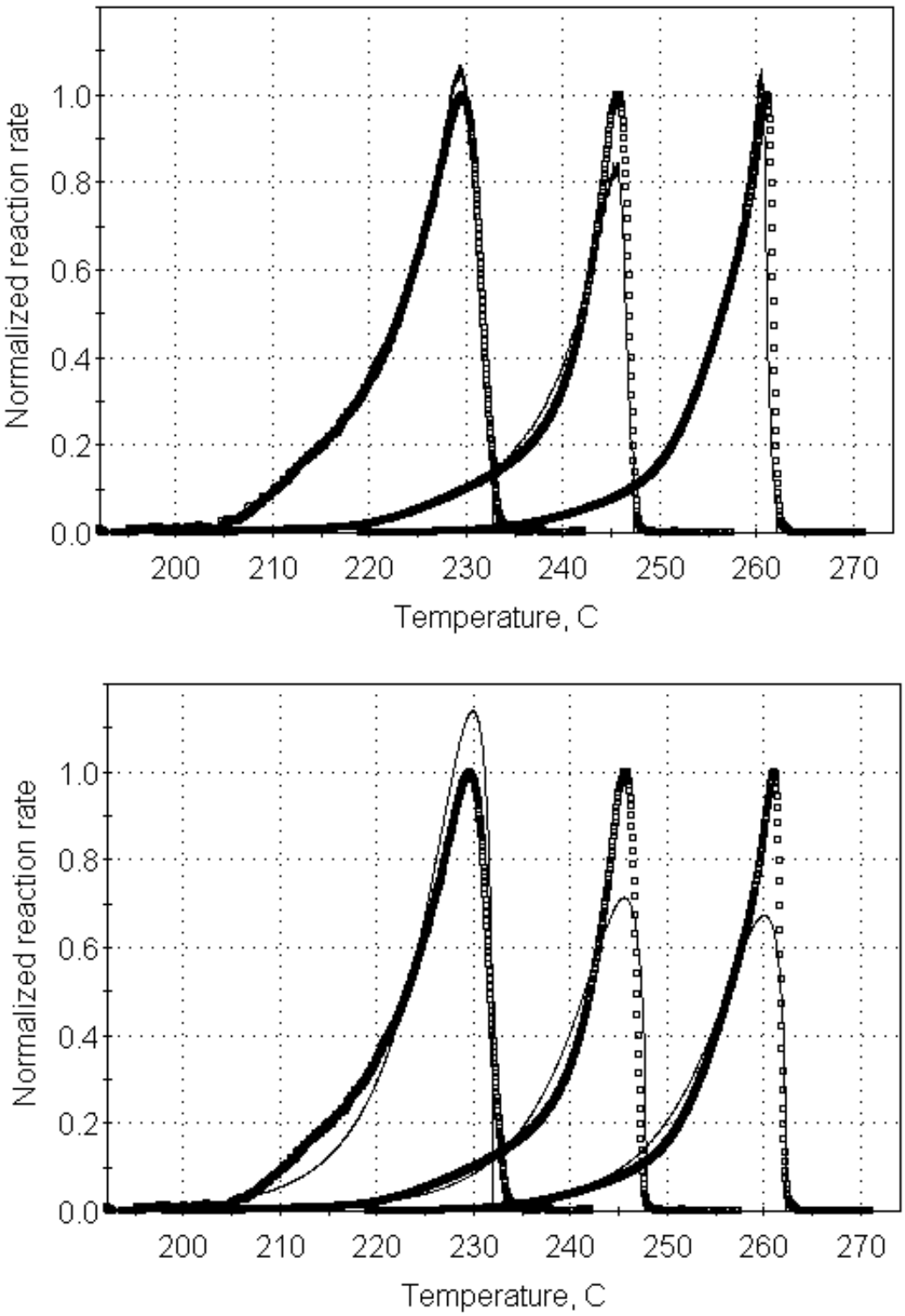

Figure 2. Comparison of the isoconversional (top) and Prout-Tompkins (bottom) models to DSC reaction rates at 0.1, 0.35, and 1.0 ^{o}C/min in a closed pan. The isoconversional model fits considerably better because of the larger number of free parameters.

HMX ODTX and STEX Modeling in ALE3D

The program ALE3D was used to model the ODTX experiment of three spherical HMX samples (½", 1", and 2" diameter) and the STEX experiment of a 2" diameter cylindrical sample. In addition, two spherical samples (1" and 2" diameter) were used in a ramped heating experiment for comparison with the cylindrical sample undergoing the STEX experiment. Isothermal simulations were performed with temperature ranges from 190°C to 335°C, while ramped simulations were performed with a range of 1°C/hr to 360°C/hr. The volume was fixed in the isothermal simulations, and the external boundaries were exposed to ambient pressure in the ramped simulations.

In these simulations, the initial temperature of the entire sample was 20°C, and the outer edge of the sample was a controlled temperature boundary condition. The "explosion" occurred when the element-averaged temperature in one element of the 50-element mesh rose rapidly due to thermal runaway. This thermal runaway rapidly decreases the simulation time step size, and the simulation terminates when the time step of the system is forced below the minimum allowable time step of 0.01 μs.

The chemical kinetics were modeled by a two-stage reaction corresponding to three HMX phases (β-HMX, δ-HMX, and HMX products). In the first stage, the β-HMX reacts to form δ-HMX in a first-order bidirectional reaction. In the second stage, both the β-HMX and δ-HMX independently react to form the products using Prout-Tompkins kinetics. Both of these reactions, in addition to an alternate model of the beta-delta phase transition, will be described later in the report.

The spherical ALE3D simulation setup contains a thin pyramidal portion of the sample with wedge angles of 4°. Periodic boundary conditions on the angled walls are assumed, and the simulation domain contains 50 elements and 204 nodes, shown in Figure 3a. For the cylindrical simulation, a two-dimensional slab was used in conjunction with the *x*-axis as an axis of rotation as shown in Figure 3b. Since the cylindrical geometry is reduced to two dimensions, a simulation of this type is often referred to ALE2D. The height of the slab is determined such that the aspect ratio of the 50 elements is unity.

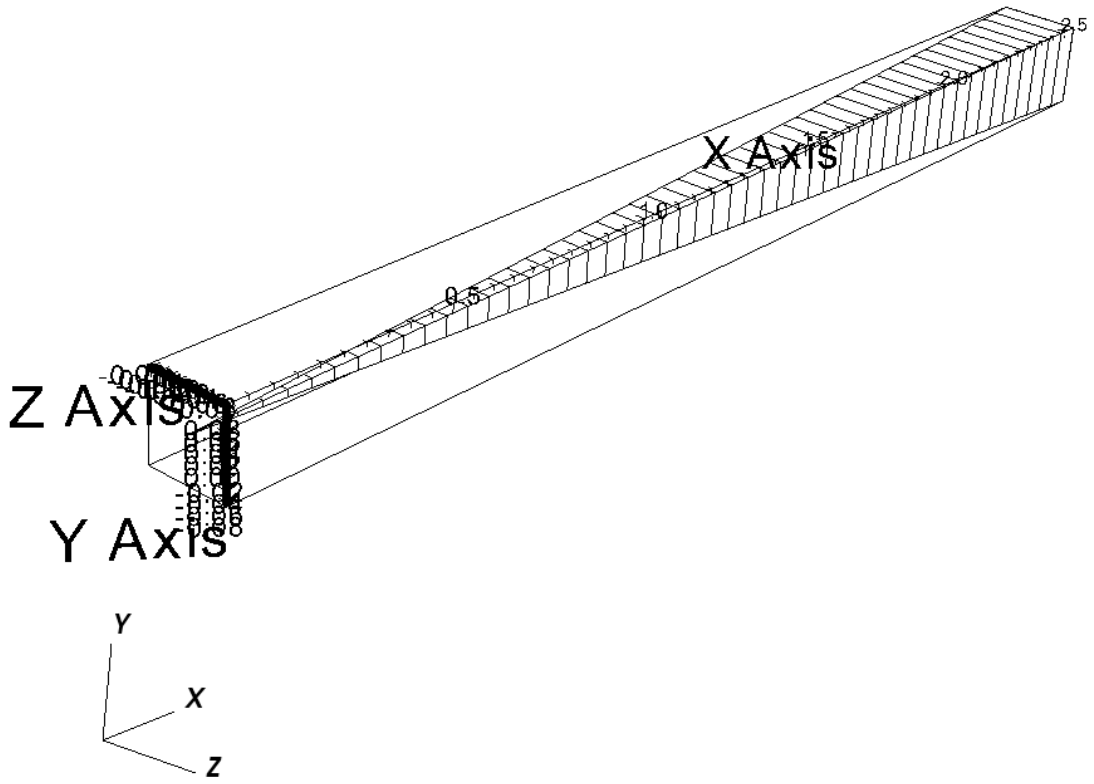

Figure 3a. Spherical mesh used in the ALE3D analysis.

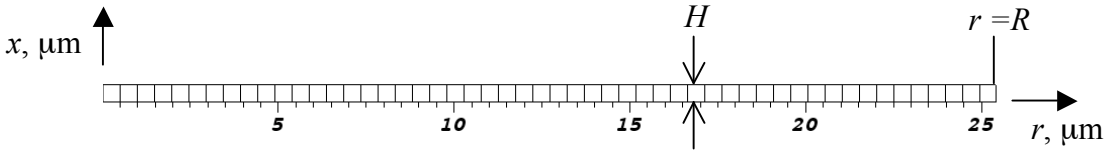

Figure 3b. Cylindrical mesh used in the ALE3D analysis.

Thermal Properties of HMX

In order to facilitate comparison of the ALE3D and AKTS codes, it was assumed that the mechanical and thermal properties of the two solid phases, β-HMX and δ-HMX, are equivalent. The thermal properties of solid HMX (heat capacity, thermal conductivity, heat of reaction) were adapted from the model of Tarver and Tran and are tabulated in Table 1 for use in the AKTS Thermal Safety program and in ALE3D. Table 1 shows property values used in both the ALE3D analysis and the AKTS Thermal Safety program. The temperature dependence of the thermal conductivity and specific heat were set to be identical in both the AKTS Thermal Safety program and ALE3D. The AKTS Thermal Safety program used a constant density for the ODTX, because it is a fixed volume, but it used a variable temperature STEX simulations the same as ALE3D. The ODTX simulations in ALE3D used a constant volume, while the variation in density for the isobaric STEX calculations in ALE3D used the 7-term polynomial equation of state for the solid HMX components.

$$P = A_0 + A_1\mu + A_2\mu^2 + A_3\mu^3 + \left(B_0 + B_1\mu + B_2\mu^2\right)E \tag{3}$$

where

$$\mu = \frac{\rho}{\rho_0} - 1$$
$$E = C_v^* T + E_{cold} \tag{4}$$

In the above equations, the coefficients A_i and B_i were previously provided by Jack Yoh for HMX, ρ_0 and C_v^* are averaged density and specific heat values, and E_{cold} is the cold energy of the material. The reference state of the materials was chosen such that the energy was zero at a temperature of 110°C and a density of 1.865 g/cm^3. Table 1 shows the density variation in the system assuming zero pressure change. Note that the density used in the AKTS Thermal Safety simulations corresponds to the density at 25°C using the equation of state in Equation (3).

In ALE3D, the gaseous products were assumed to contain the same properties as a gamma-law gas. This introduces a small difference in the time to explosion from AKTS calculations, because the AKTS code assumes the same thermal properties for all materials in a given region. The gamma-gas law is given by

$$P = \left(\gamma - 1\right)\frac{\rho}{\rho_0}E \tag{5}$$

where $\gamma = 1.283$. The reference state used was 500°C and 1.865 g/cm^3. The product gases contained temperature-independent thermal properties: thermal conductivity = 0.0004188 W/cm/K, density = 1.865 g/cm^3, and specific heat = 1.422 J/g/K.

A heat transfer coefficient of 10 W/cm^2/K was used in the AKTS program, which is nearly equivalent to assuming that the outside surface is at the heat bath temperature:

- The surface temperature of a semi-infinite medium exposed to external convection is (Incropera and Dewitt, 1996),

$$\frac{T(0,t)-T_i}{T_\infty - T_i} = 1 - \exp(\xi^2)\mathrm{erfc}(\xi), \text{where } \xi = \frac{h\sqrt{\alpha t}}{k} \tag{6}$$

  where h is the heat transfer coefficient, α is the thermal diffusivity, t is time, k is thermal conductivity, and T_i and T_∞ are the initial and applied external temperatures, respectively.

- The right-hand side of the above equation is unity for $\xi > 6$. Therefore, using the material properties provided in Table 1, the surface temperature is equivalent to the external applied temperature for $t > 10$ ms. It will be shown later that this time is small compared to that for the overall ODTX experiment, and hence the assumption of the equivalence to a constant temperature boundary condition is justified for this analysis.

The temperature of the external boundary nodes was controlled directly in the ALE3D simulations. The AKTS Thermal Safety program used a heat of reaction of -1335 cal/g, while the enthalpy of formation values of δ-HMX and the product gases in ALE3D were specified as 7.9 cal/g and -1337 cal/g, respectively.

Table 1. Thermal properties of solid HMX used in ALE3D and the AKTS Thermal Safety program.

Temperature, ^{o}C	Thermal conductivity, W/cm/K		Density,* g/cm^3		Specific heat, J/g/K	
	ODTX	STEX	ODTX	STEX	ODTX	STEX
25	0.0053	0.0053	1.892	1.892	1.004	1.004
75	0.0051	0.0051	1.892	1.879	1.172	1.172
125	0.0049	0.0049	1.892	1.866	1.339	1.339
160	0.0046	0.0046	1.892	1.856	1.422	1.422
180	0.0044	0.0044	1.892	1.850	1.464	1.464
225	0.0041	0.0041	1.892	1.836	1.548	1.548
275	0.0039	0.0039	1.892	1.820	1.632	1.632

*The ODTX calculations used a fixed volume, hence a fixed density of 1.892 g/ cm^3, while the isobaric STEX calculations used this dependence of density on temperature.

Chemical Kinetics Model

The sample is initially comprised of 100% β-HMX. At time $t = 0$, the external boundary is maintained at either a constant (isothermal case) or ramped temperature, warming the sample over time. When the temperature of an element is sufficient, the β-HMX transitions to δ-HMX. This transition may be modeled according to the single bidirectional reaction,

$$\beta \xrightarrow{k_1} \delta \tag{7}$$

This reaction sequence results in changes in mass fractions as

$$\begin{aligned} \frac{dx_\beta}{dt} &= -k_1\left(T, x_\beta\right) \\ \frac{dx_\delta}{dt} &= +k_1\left(T, x_\beta\right) \end{aligned} \tag{8}$$

where x_β and x_δ are the mass fractions of β-HMX and δ-HMX, respectively, and k_1 is the reaction rate

$$k_1\left(T, N_\beta\right) = A_1 x_\beta \exp\left(-\frac{E_1}{RT}\right)\sinh\left(\Lambda_{e,1}^* - \frac{E_{e,1}^*}{RT}\right) \tag{9}$$

where the values of the parameters used are

$$\begin{aligned} E_1/R &= 29100 \text{ K} \\ A_1 &= 2.072 \times 10^{26} \text{s}^{-1} \\ E_{e,1}^*/R &= 1182.7 \text{ K} \\ \Lambda_{e,1}^* &= 2.6247 \end{aligned} \tag{10}$$

Note that the sinh function in Equation (9) is an approximation to the model proposed by Burnham (2004),

$$k\left(N,T\right) = A x^a \exp\left(-\frac{E^*}{RT}\right)\left(1 - 1/K_{eq}\right) \tag{11}$$

where K_{eq} is the equilibrium constant. A similar temperature dependence of Equations (9) and (11) may be found by setting both to zero at an equilibrium temperature T_{eq}:

$$\sinh\left(\Lambda_e^* - \frac{E_e^*}{RT_{eq}}\right) = 1 - \frac{1}{K_o \exp\left(-\frac{E_e^*}{RT_{eq}}\right)} \tag{12}$$

The two functional relations may be compared using

$$\Lambda_e^* = \frac{E_e^*}{RT_{eq}} = \ln K_o$$
$$E_e^* = \Lambda_e^* RT_{eq} \tag{13}$$

for known values of T_{eq} and K_o. In this study, the values of T_{eq} and K_o used were 177.4°C and 13.8, respectively.

The second part of the reaction involves the Prout-Tompkins-based transitioning of both β-HMX and δ-HMX to gaseous products,

$$\beta \xrightarrow{k_{2a}} p$$
$$\delta \xrightarrow{k_{2b}} p \tag{14}$$

This reaction sequence results in changes in mass fractions as

$$\frac{dx_\beta}{dt} = -k_{2a}\left(T, x_\beta, x_S\right)$$
$$\frac{dx_\delta}{dt} = -k_{2b}\left(T, x_\delta, x_S\right) \tag{15}$$
$$\frac{dx_p}{dt} = +k_{2a}\left(T, x_\beta, x_S\right) + k_{2b}\left(T, x_\delta, x_S\right)$$

where x_p is the mass fraction of products, and x_S is the combined mass fractions of the solid phases,

$$x_S = x_\beta + x_\delta \tag{16}$$

which was implemented using ALE3D's pseudospecies capability. The reaction rates k_{2a} and k_{2b} are calculated as

$$k_{2a}\left(T, x_\beta, x_S\right) = A_{2a} \exp\left(-\frac{E_{2a}}{RT}\right) x_\beta^n \left[1 - q x_S\right]^m$$
$$k_{2b}\left(T, x_\delta, x_S\right) = A_{2b} \exp\left(-\frac{E_{2b}}{RT}\right) x_\delta^n \left[1 - q x_S\right]^m \tag{17}$$

The values of the parameters used in the above reaction are

$$
\begin{aligned}
n &= 0.320 \\
m &= 0.635 \\
q &= 0.99 \\
A_{2a} &= A_{2b} = 3.81 \times 10^{13}\,\mathrm{s}^{-1} \\
E/R &= 19775\ \mathrm{K}
\end{aligned}
\tag{18}
$$

Note that the ALE3D input parameter *rhopow* = 1 - *m* - *n* was applied in the above Prout-Tompkins reactions to change the reaction from the default mass concentration basis to a mass fraction basis. In addition, since the beta-delta phase transition follows a first order bidirectional reaction, no application of *rhopow* was necessary to convert to a mass fraction basis.

Isothermal Time-to-Explosion Calculations

Results from ODTX simulations for a ½"-diameter spherical sample are shown in Figure 4 using both the AKTS Thermal Safety Program and ALE3D. The reasonable agreement between the three sets of data suggests that the kinetics of the ALE3D model are behaving correctly. However, the ALE3D simulations suggest a slightly more rapid explosion than the AKTS simulations at low temperatures. The reason for this disagreement may be attributed to the lower thermal diffusivity of the products phase in ALE3D compared to that used in the AKTS simulations, because at low temperatures the mass fraction of the products becomes significant enough to affect the dissipation of heat from the active site. AKTS has only a single phase for calculating thermal transport, while ALE3D has separate parameters for the solid and gas phases. It should be noted that HMX has a melting point at 280°C, but the solid-liquid phase transition was not incorporated into the simulations.

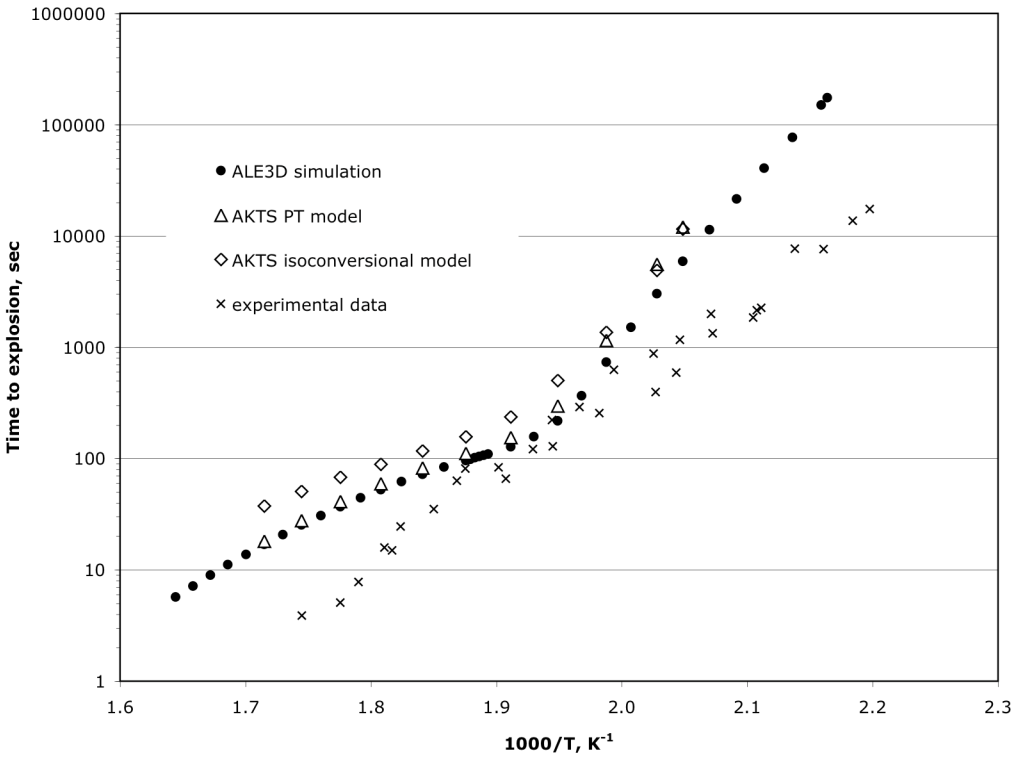

Figure 4. Experimental and simulated ½" diameter ODTX times.

Figure 4 also shows experimental data collected for the ½"-diameter ODTX setup for comparison with the simulation results. There appears to be good agreement between ALE3D simulation and experimental results between 220°C and 265°C. However, the simulated ODTX data in Figure 4 show a bend in their respective trends, which is not consistent with experimental ODTX results. Both ALE3D and the AKTS code predicts that this bend occurs at approximately 1000/T = 1.95 (T ~ 240°C). This transition may be related to the location of thermal runaway in the sample. For temperatures above this transition, thermal runaway occurs at the outer edge of the sphere, while for lower temperatures, thermal runaway occurs at the center of the sphere. Figure 5 shows the location of the explosion in the sample as a function of the surface temperature. Note that the location of the transition in Figure 4 roughly corresponds to the highest temperature at which the explosion occurs at the center of the sample. The AKTS Thermal Safety code predicts that the maximum temperature for thermal runaway at the center of the sample is 255°C for the Prout-Tompkins model and 260°C for the isoconversional model. Figure 5 shows that ALE3D predicts that this temperature is 245°C.

Given the disagreements in Figure 4 between measurement and calculation, we note that the primary purpose of the work to date was not to optimize the thermal parameters, but rather to characterize and compare the various approaches with kinetics calibrated by DSC. It has been observed elsewhere that DSC kinetics are too slow to predict times to

explosion for macroscopic samples (Erikson, 2005), and that issue will be explored in follow-up work.

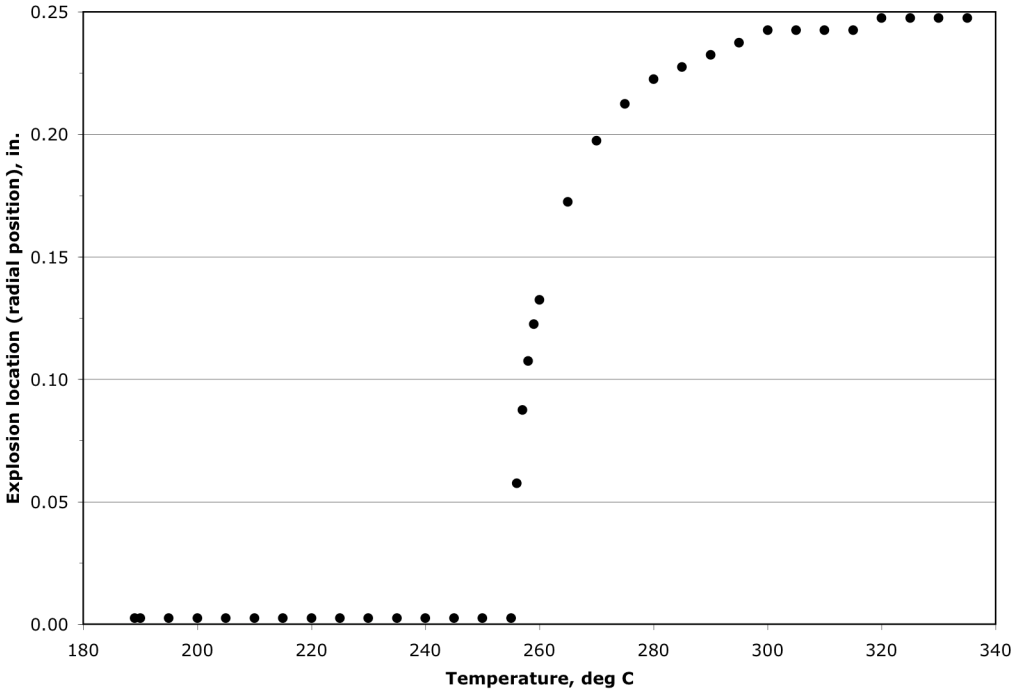

Figure 5. Explosion location in ½" diameter spherical sample, isothermal case.

Figure 5 depicts that for temperatures below 255°C, thermal runaway occurs at the center of the sample, while for temperatures above 320°C, thermal runaway occurs at the outer edge of the sample. Therefore, histories of the element-averaged temperature and species mass fractions were taken for various elements in the domain for the 195°C and the 330°C cases, which correspond to the two limits at which thermal runaway occurs.

The history plots of temperature, β-HMX mass fraction, δ-HMX mass fraction, and HMX products mass fraction are shown in Figures 6a, 6b, 6c, and 6d, respectively for a ½" diameter ODTX setup at 330°C. The temperature history plot clearly shows thermal runaway occurring at 7.2 seconds in the outwardmost element only. Figures 6a and 6b show that the β-HMX→δ-HMX transition follows a defined boundary that moves towards the center of the sphere (i.e., shrinking core reaction). Figure 6c also shows that the amount of δ-HMX present near the outer edge of the sphere reduces with time late in the simulation, suggesting the reaction to product gases. This suggestion is further justified by the increase in reacted products shown by Figure 6d.

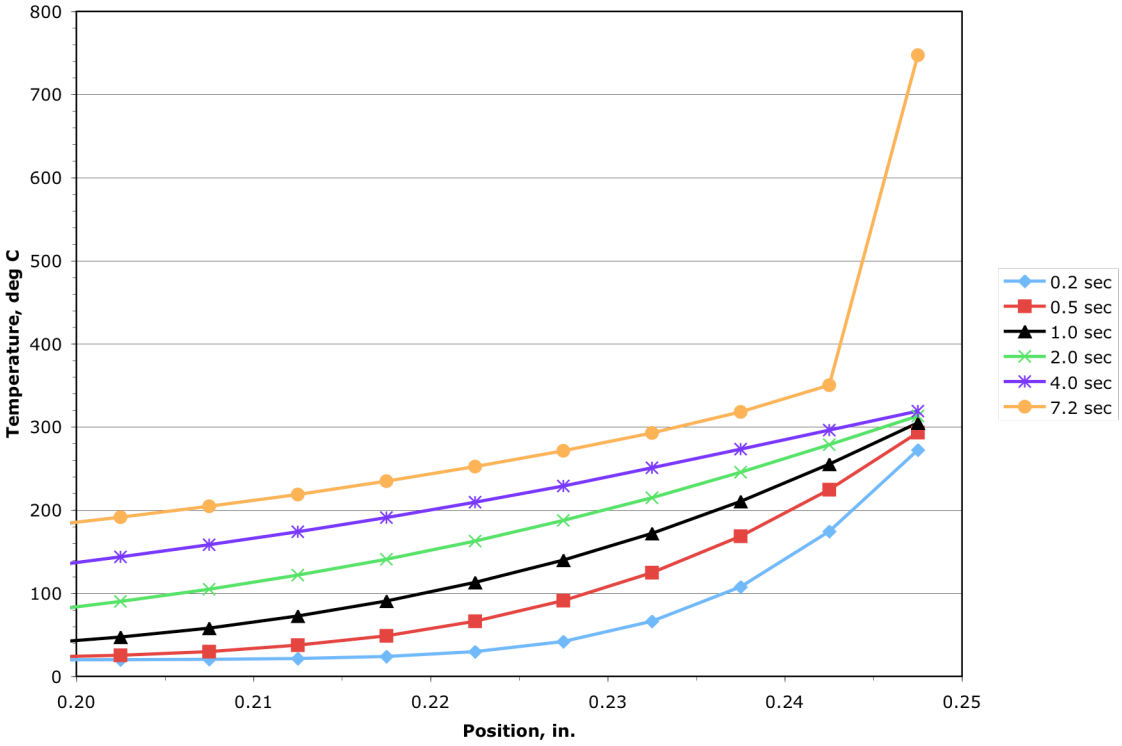

Figure 6a. Temperature history of ½" diameter ODTX, 330°C case.

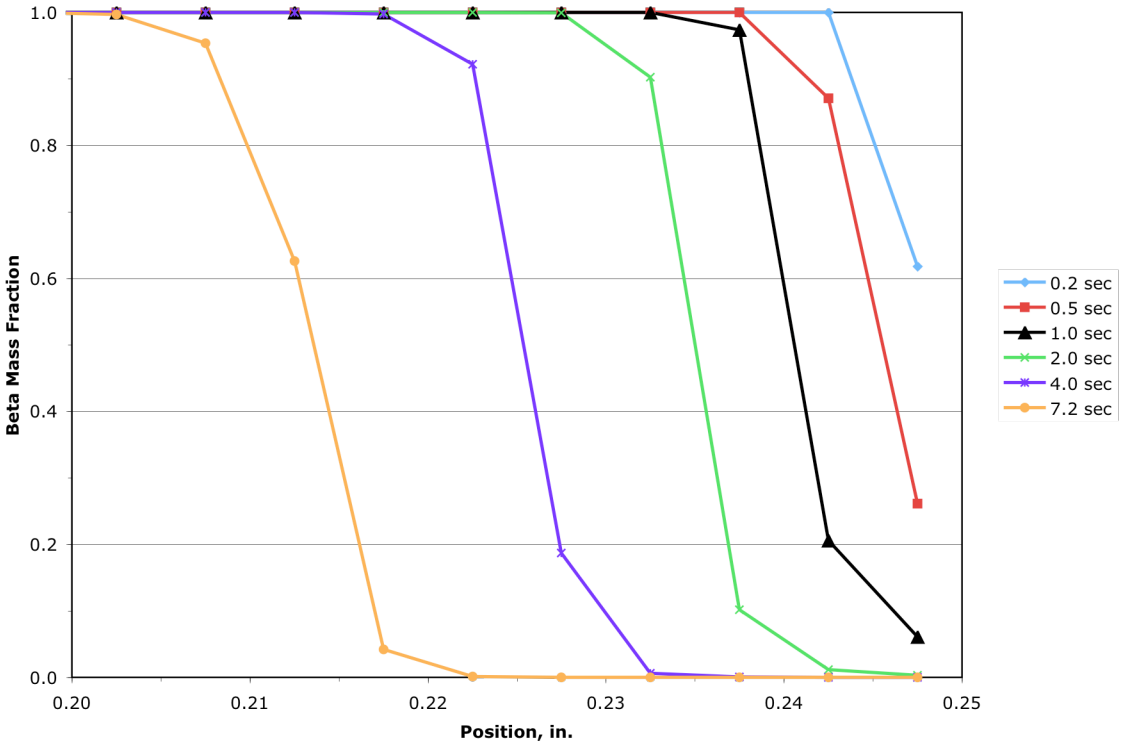

Figure 6b. β-HMX mass fraction history of ½" diameter ODTX, 330°C case.

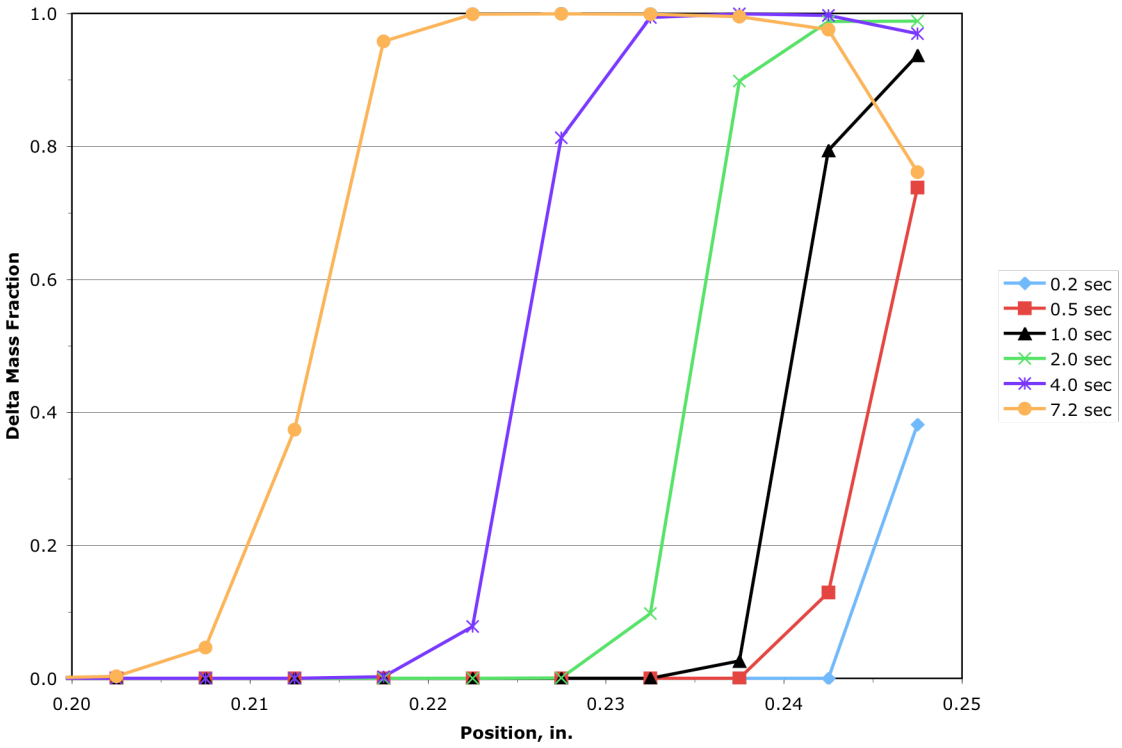

Figure 6c. δ-HMX mass fraction history of ½" diameter ODTX, 330°C case.

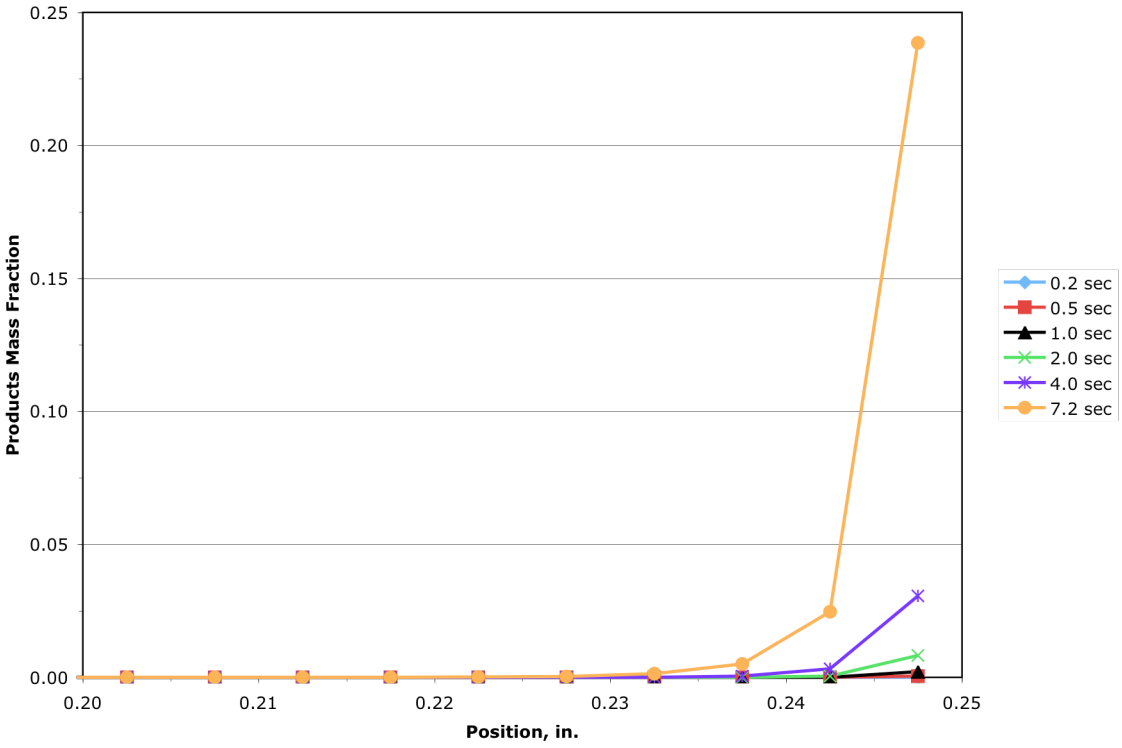

Figure 6d. HMX products mass fraction history of ½" diameter ODTX, 330°C case.

The histories of temperature and species mass fraction were also determined for a ½" diameter 195°C ODTX setup. These histories are plotted in Figures 7a, 7b, 7c, and 7d. Figure 7a shows that the thermal runaway occurs at 21.4 hours near the center of the sphere. Figures 7b and 7c show that the β-HMX→δ-HMX transition does not appear to be a sharp boundary as in Figure 6b, but rather a gradual one (i.e., close to a volumetrically uniform reaction). Due to the longer thermal diffusion path from the center, the sphere eventually becomes hotter in the center, and there are more gaseous products in the center at the time of thermal runaway, as shown in Figure 7d. In fact, the mass fraction of products at the center of the sphere approaches 70% before thermal runaway occurs.

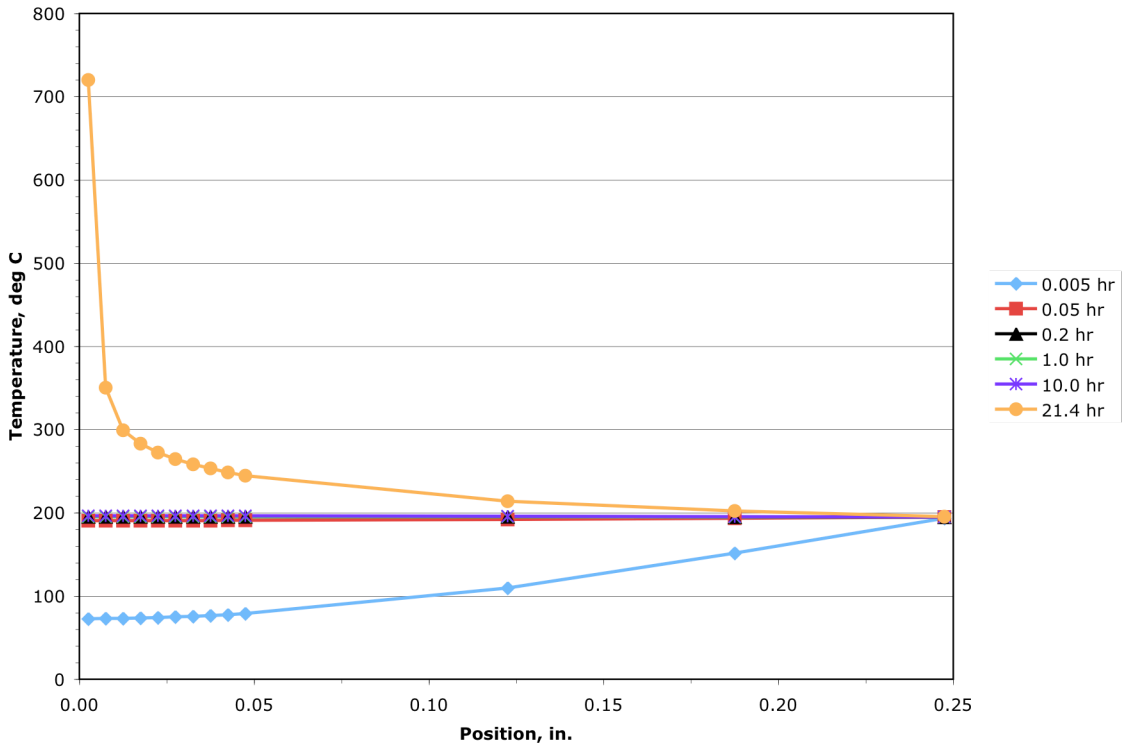

Figure 7a. Temperature history of ½" diameter ODTX, 195°C case.

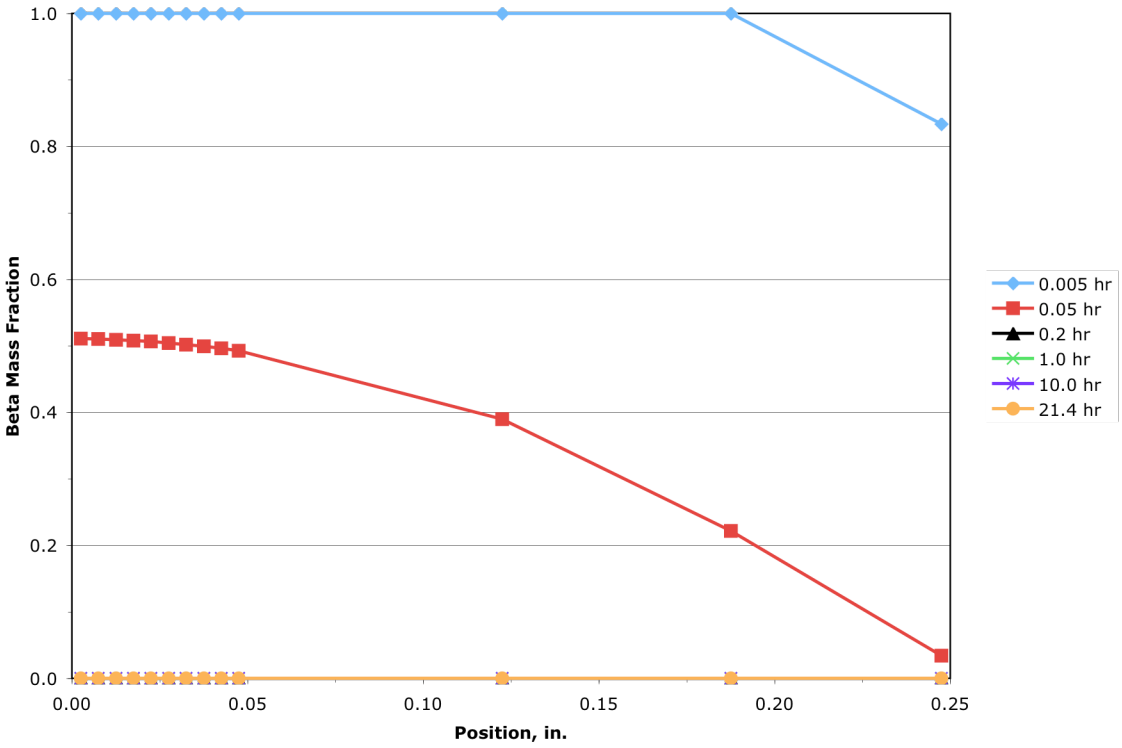

Figure 7b. β-HMX mass fraction history of ½" diameter ODTX, 195°C case.

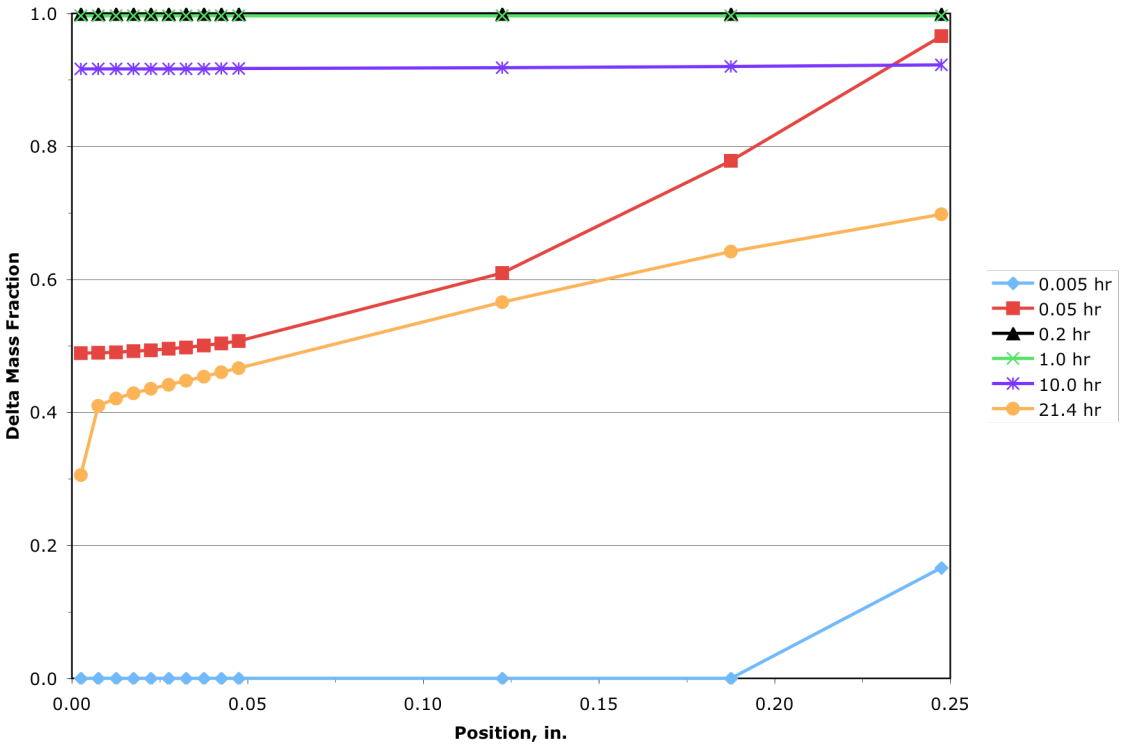

Figure 7c. δ-HMX mass fraction history of ½" diameter ODTX, 195°C case.

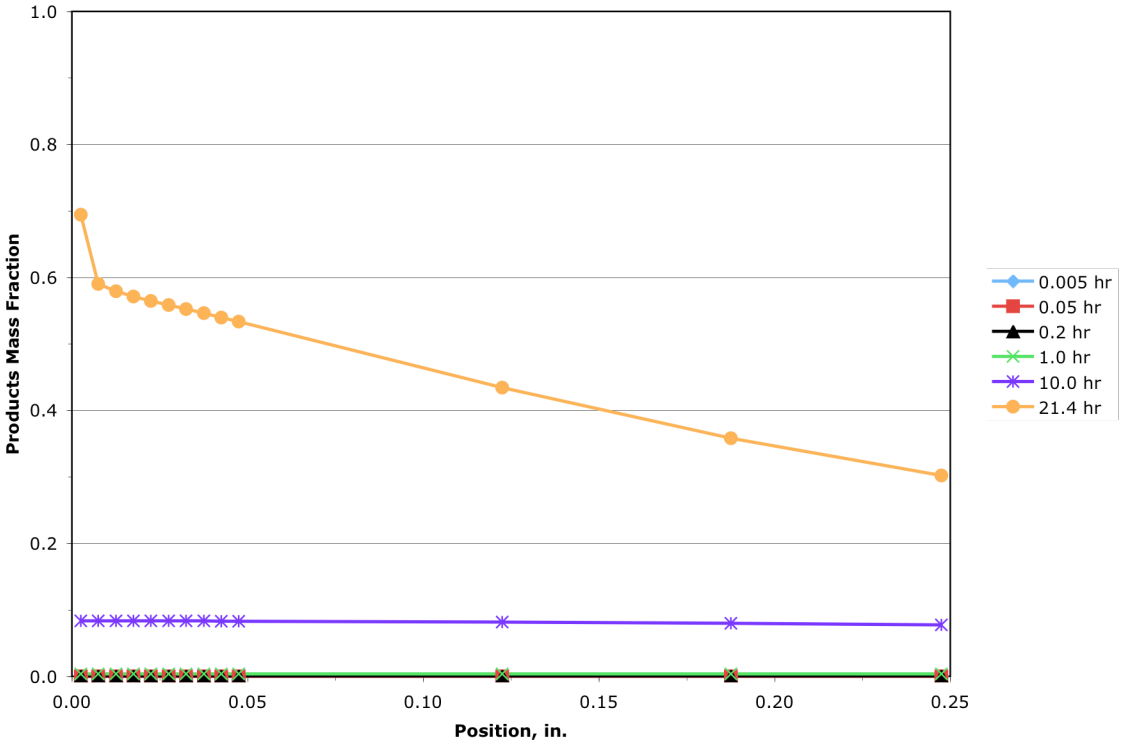

Figure 7d. HMX products mass fraction history of ½" diameter ODTX, 195°C case.

Theoretical Validation

The curves in Figure 6a suggest that conduction may dominate for small values of time. These curves may be compared to a theoretical derivation of temperature for pure conduction. In this derivation, the temperature of a solid sphere with a fixed outer temperature may be written as

$$\begin{aligned} &\frac{1}{r}\frac{\partial^2}{\partial r^2}(rT) = \frac{1}{\alpha}\frac{\partial T}{\partial t} \\ &\frac{\partial T}{\partial r} = 0, \qquad r = 0, t > 0 \\ &T = T_o, \qquad r = b, t > 0 \\ &T = T_i, \quad 0 < r < b, t = 0 \end{aligned} \tag{19}$$

where α is the thermal diffusivity of β-HMX, b is the outer radius of the sphere, T_o is the fixed outer temperature of the sphere, and the sphere is initially at a uniform temperature

T_i. Performing the substitution $U \equiv rT$ simplifies Equation (19) into the form (Ozisik, 1980),

$$\begin{aligned}
&\frac{\partial^2 U}{\partial r^2} = \frac{1}{\alpha}\frac{\partial U}{\partial t} \\
&U = 0, \quad r = 0, t > 0 \\
&U = bT_o, \quad r = b, t > 0 \\
&U = rT_i, \quad 0 < r < b, t = 0
\end{aligned} \tag{20}$$

Equation (20) may be split up into a steady-state and homogeneous solution,

$$U(r,t) = U_s(r) + U_h(r,t) \tag{21}$$

where $U_s = rT_o$, and

$$\begin{aligned}
&\frac{\partial^2 U_h}{\partial r^2} = \frac{1}{\alpha}\frac{\partial U_h}{\partial t} \\
&U_h = 0, \quad r = 0, t > 0 \\
&U_h = 0, \quad r = b, t > 0 \\
&U_h = r(T_i - T_o), \quad t = 0, 0 < r < b
\end{aligned} \tag{22}$$

The solution to Equation (22) is known from separation of variables to be (Ozisik, 1980)

$$U_h(r,t) = \frac{2(T_i - T_o)}{b}\sum_{n=1}^{\infty}\sin\left(\frac{n\pi r}{b}\right)\exp\left(-\alpha\left(\frac{n\pi}{b}\right)^2 t\right)\int_0^b \hat{r}\sin\left(\frac{n\pi\hat{r}}{b}\right)d\hat{r} \tag{23}$$

The integral in the above equation may be simplified as

$$\int_0^b \hat{r}\sin\left(\frac{n\pi\hat{r}}{b}\right)d\hat{r} = \frac{b^2}{n\pi}(-1)^{n+1} \tag{24}$$

Combining Equations (21), (22), and (23) yields

$$\frac{T(r,t) - T_o}{T_i - T_o} = \begin{cases} \dfrac{2}{r}\displaystyle\sum_{n=1}^{\infty}\frac{(-1)^{n+1}}{(n\pi/b)}\sin\left(\frac{n\pi r}{b}\right)\exp\left(-\alpha\left(\frac{n\pi}{b}\right)^2 t\right), & r > 0 \\ 2\displaystyle\sum_{n=1}^{\infty}(-1)^{n+1}\exp\left(-\alpha\left(\frac{n\pi}{b}\right)^2 t\right), & r = 0 \end{cases} \tag{25}$$

The simulation data are plotted against the theoretical results for 300°C in Figure 8a, where the thermal properties were taken for 125°C from Table 1. In the simulations, all values of heat of formation were set to zero to negate any heat generation due to

chemistry. Note that the 300°C ODTX case also features negligible products mass fraction values over the time range given. The curves show good agreement with simulation data, which suggests that the code is working properly. The slight disagreement between simulation data and the curves may be attributed to the errors in the code's thermal convergence criteria and the cutoff in the number of terms used in the analytical solution.

Figure 8b also shows the influence of chemistry in the aforementioned simulation by comparing temperature curves where the heats of formation are nonzero to curves where the heats of formation are zero. Note that for a position greater than 0.21 in. for times larger than 2 seconds, the nonzero heat of formation data tend to be below the zero heat of formation results, which suggests the influence of the β-HMX→δ-HMX endothermic reaction. It can clearly be seen that conduction is the dominant mode of heat transfer for the majority of the simulation, and the thermal runaway doesn't occur until the temperature is in the range of the DSC measurement. In contrast, for runaway heating in the center of the sample, the ability of the sample to generate heat faster than it is conducted away becomes particularly important, and how fast the reaction quenches (i.e., the activation energy) becomes very important for the low-temperature extrapolation.

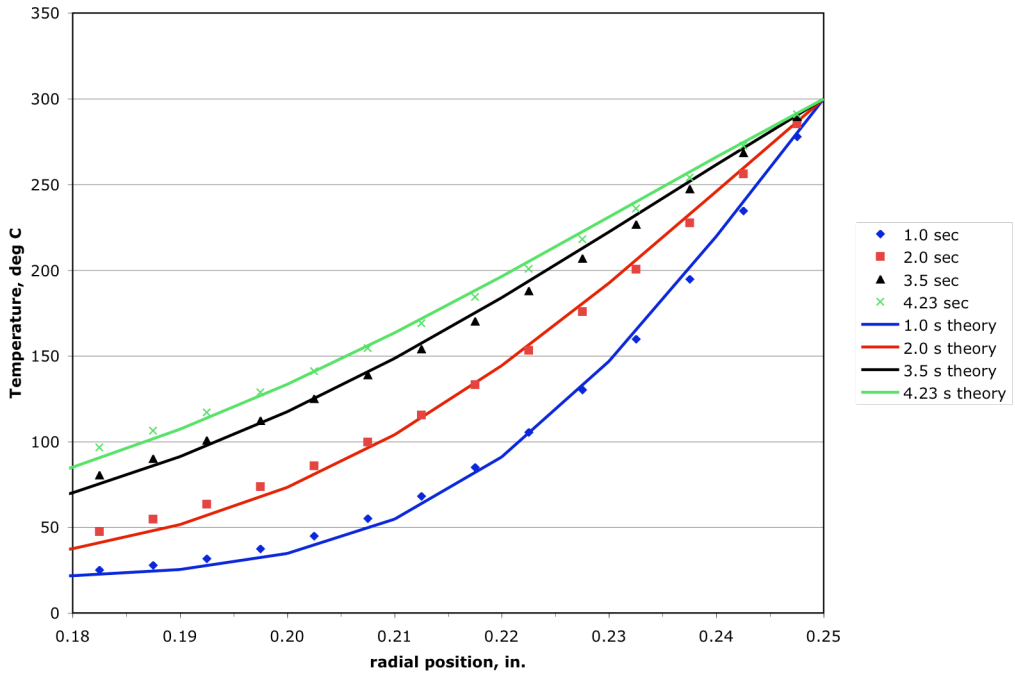

Figure 8a. Comparison of simulation data to conduction-only theoretical results where heats of formation are set to zero, 300°C case.

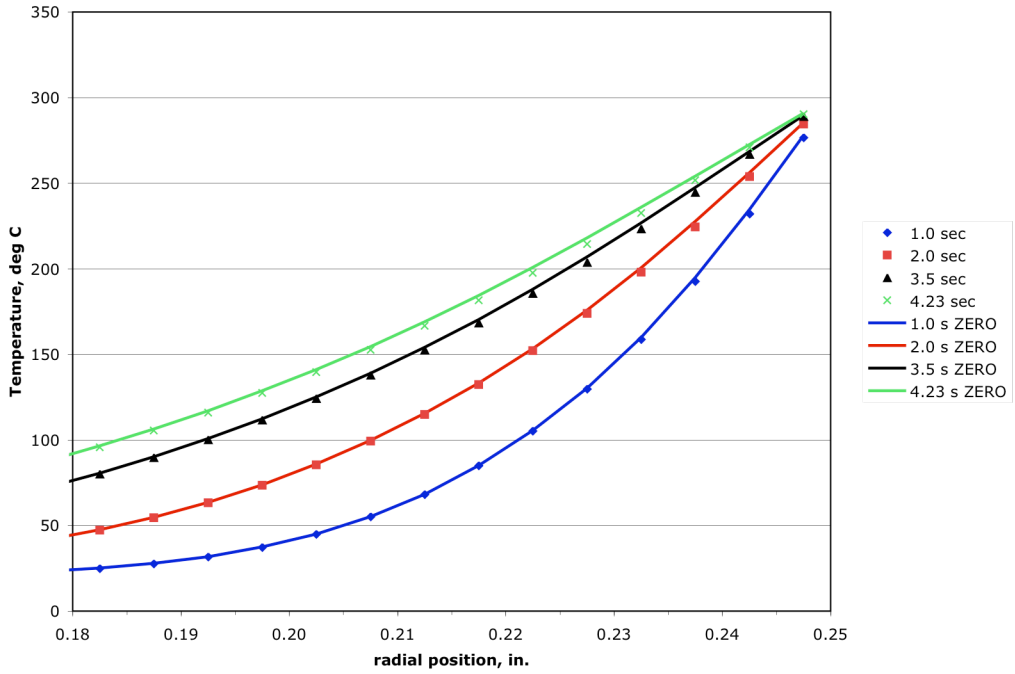

Figure 8b. Comparison of simulation data where heats of formation are zero and nonzero to show the effects of the β-HMX→δ-HMX endothermic reaction, 300°C case.

Effects of Beta-Delta Phase Transition Kinetics on ODTX Simulations

The above results were based on the single-reaction bidirectional beta-delta phase transition in Equation (9). However, other models for the phase transition are available. Henson et al. (2002) developed a reversible autocatalytic kinetics model, while Wemhoff and Burnham (2006) developed three bidirectional autocatalytic kinetics models. In this study, the simplest of these four models, a two-reaction bidirectional autocatalytic model, is used for comparison to the single bidirectional model. The two-reaction bidirectional autocatalytic model follows

$$\begin{aligned} \beta &\xrightarrow{k_{1a}} \delta \\ \beta + \delta &\xrightarrow{k_{1b}} 2\delta \end{aligned} \tag{26}$$

This reaction sequence results in changes in mass fractions as

$$\begin{aligned} \frac{dx_\beta}{dt} &= -k_{1a}\left(T, x_\beta\right) - k_{1b}\left(T, x_\beta, x_\delta\right) \\ \frac{dx_\delta}{dt} &= +k_{1a}\left(T, x_\beta\right) + k_{1b}\left(T, x_\beta, x_\delta\right) \end{aligned} \tag{27}$$

where x_β and x_δ are the mass fractions of β-HMX and δ-HMX, respectively, and k_{1a} and k_{1b} are the reaction rates

$$k_{1a}\left(T,x_\beta\right) = A_{1a}x_\beta \exp\left(-\frac{E_{1a}}{RT}\right)\sinh\left(\Lambda^*_{e,1a} - \frac{E^*_{e,1a}}{RT}\right)$$
$$k_{1b}\left(T,x_\beta,x_\delta\right) = A_{1b}x_\beta x_\delta \exp\left(-\frac{E_{1b}}{RT}\right)\sinh\left(\Lambda^*_{e,1b} - \frac{E^*_{e,1b}}{RT}\right) \quad (28)$$

where the values of the parameters used are

$$E_{1a}/R = 38817 \text{ K}$$
$$E_{1b}/R = 3522.9 \text{ K}$$
$$E^*_{e,1a}/R = E^*_{e,1b}/R = 1181.6 \text{ K} \quad (29)$$
$$\Lambda^*_{e,1a} = \Lambda^*_{e,1b} = 2.728$$

The values of $\Lambda^*_{e,1a} = \Lambda^*_{e,1b}$ and $E^*_{e,1a} = E^*_{e,1b}$ were derived using Equation (13), where the parameters T_{eq} and K_o are 160°C and 15.3, respectively. Two sets of parameters A_{1a} and A_{1b} were previously calibrated to match data from either 165°C X-ray diffraction (XRD) experiments (Zaug et al., 2003) or from the Sandia Instrumented Thermal Ignition (SITI) experiment (Kaneshige et al., 2002):

- Parameters calibrated using 165° XRD basis:
  $A^0_{1a} = 1.0 \times 10^{34}\,\text{s}^{-1}$
  $A^0_{1b} = 3.0 \times 10^{1}\,\text{s}^{-1}$

- Parameters calibrated using SITI basis:
  $A^0_{1a} = 1.0 \times 10^{34}\,\text{s}^{-1}$
  $A^0_{1b} = 4.0 \times 10^{2}\,\text{s}^{-1}$

The ALE3D ODTX simulations were run using the two-reaction bidirectional autocatalytic model for comparison to the single bidirectional data shown in Figure 4. Figure 9 shows that the effects of the phase transition model are negligible for most temperatures. However, the data for the two-reaction model using the 165°C XRD-based parameters deviates from the other models slightly from 1000/T = 2.0 to 2.1. The cause of this deviation may stem from the type of material present in the decomposition reactions. For the two-reaction model using 165°C XRD-based parameters, at 220°C both β-HMX and δ-HMX decompose to form gas products, while only the δ-HMX decomposes at that temperature when the other models are used.

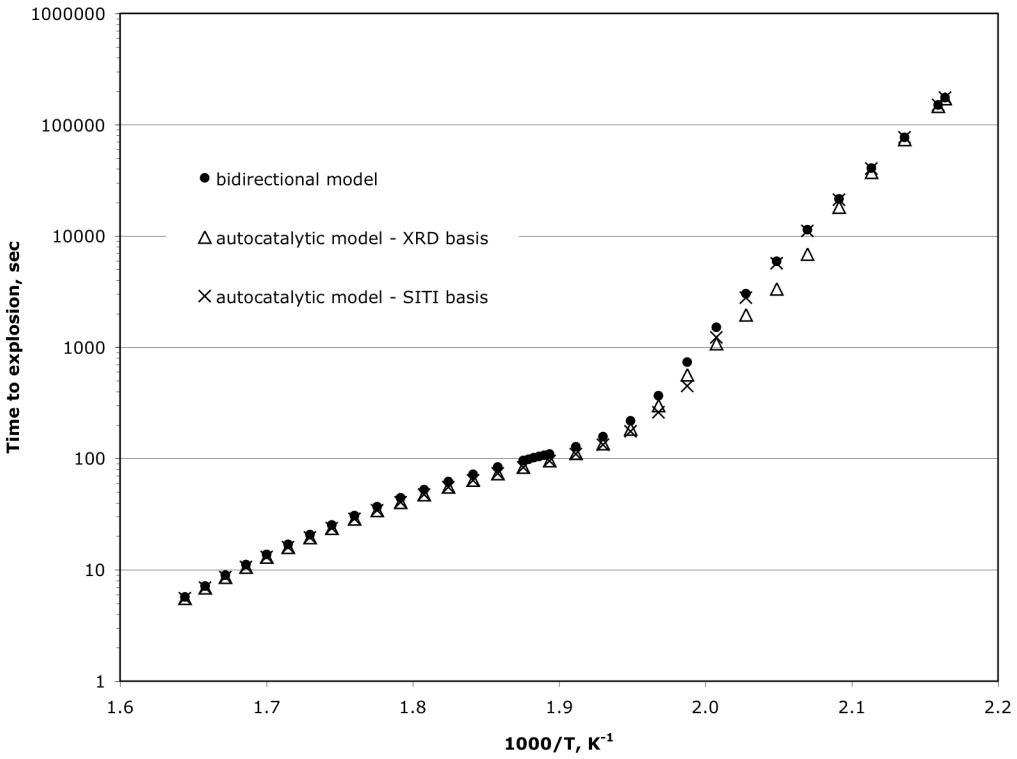

Figure 9. Comparison of ODTX simulation data based on beta-delta phase transition kinetics.

Effects of Sample Diameter

The effects of adjusting the sample diameter to 2" were also investigated. Figure 10 shows that this adjustment changes the effect on the time to explosion, for the curve undergoes less of a bend in data for the temperature range given, which means that explosions in the 2" diameter sample occur faster at lower temperatures compared to the ½" diameter sample, while the opposite is true at higher temperatures. The 'cross-over' temperature at which this occurs is approximately 225°C.

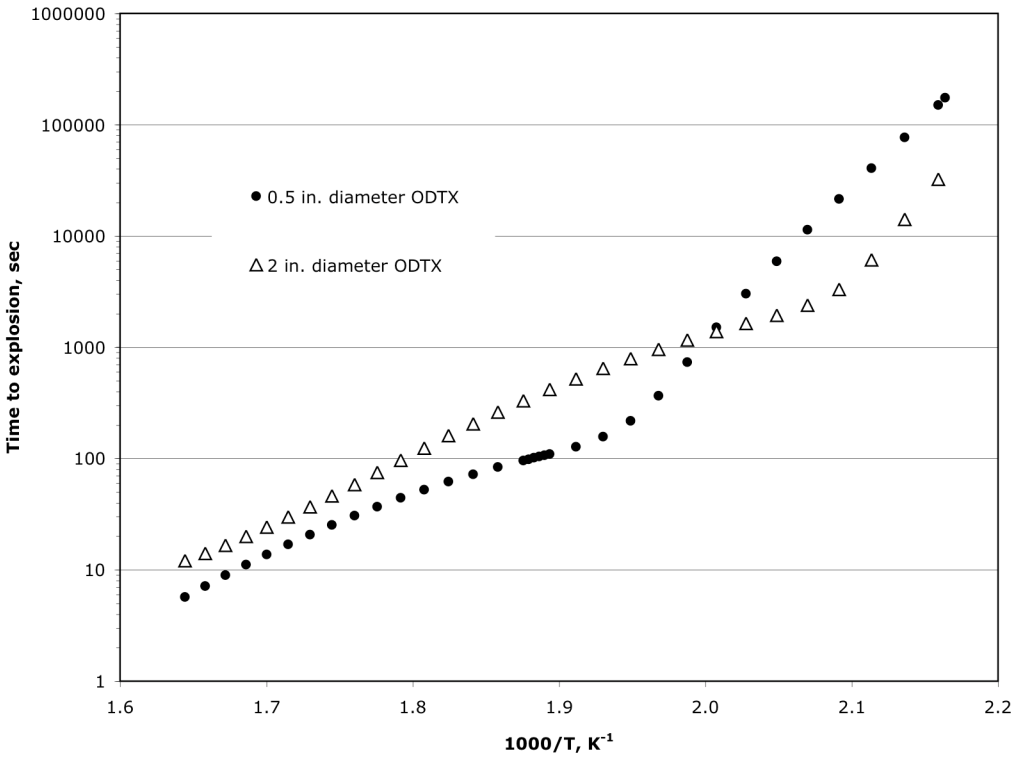

Figure 10. Effects of sample diameter on time to explosion.

Cylindrical Geometry

Isothermal simulation runs were also performed for a 2" diameter cylindrical sample corresponding to the grid of Figure 3b. The results are compared to the 2" ODTX sample in Figure 11. The figure shows that the times to explosion are similar for the cylinder and sphere for the isothermal case, but a crossover occurs at approximately 203°C, where the cylinder has a slightly lower time to explosion at low temperatures.

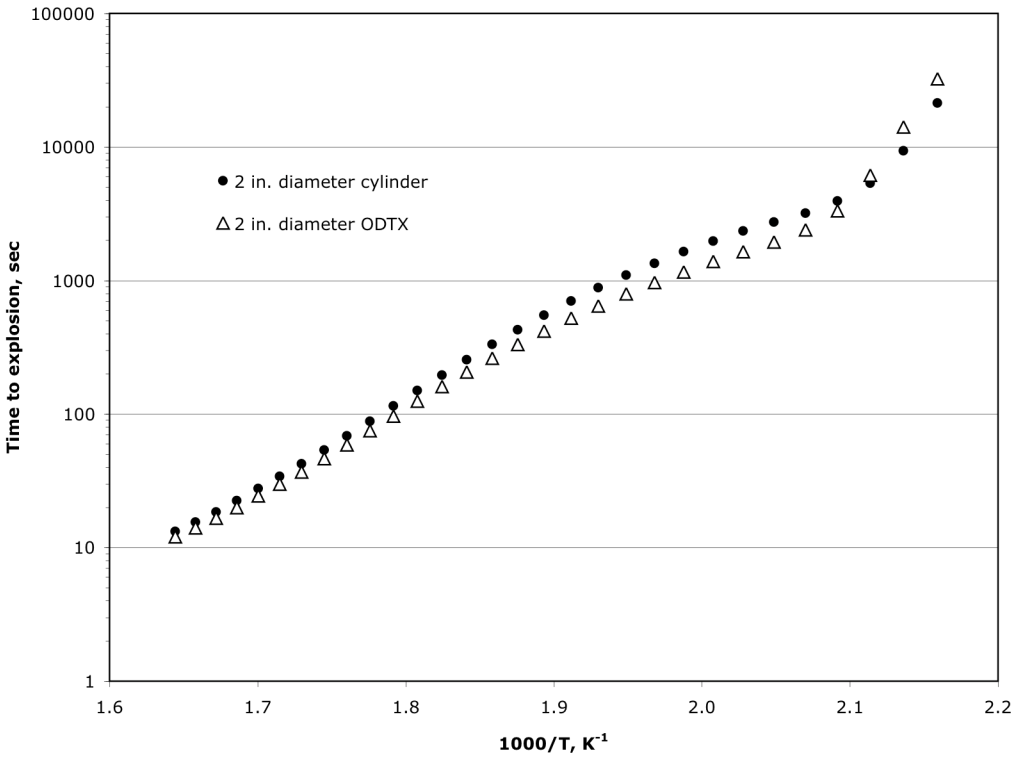

Figure 11. Time to explosion for isothermal 2" diameter cylindrical and spherical geometries.

Ramped Heating

The 2"-diameter STEX and 1"-diameter and 2"-diameter spherical samples were used in ramped heating simulations. In these simulations, the boundary temperature was raised at a constant rate over time from a starting point of 20°C. The nodal temperature histories at the outer boundary confirmed the appropriate ramping of the boundary temperature. Results are shown in Figures 12a and 12b for ramp rates from 1°C/hr to 360°C/hr. In addition, results are provided for 2"-diameter STEX AKTS Thermal Safety simulations using the isoconversional and Prout-Tompkins models. Figure 12a shows that the time to explosion follows a power-law relationship with the ramping rate, and the time to explosion is nearly independent on size and geometry for the samples shown. In contrast, there is a notable difference in explosion time for isothermal boundary conditions. Figure 12b shows a cross-over in data for all three models, where the cylindrical geometry provides the steepest time-temperature relationship. The slight discontinuity in the 1" diameter data shown around 140°C/hr can be attributed to numerical convergence tolerance. Finally, both figures show good agreement between the 2" diameter STEX simulations at 1°C/hr by the AKTS Thermal Safety program and ALE3D Prout-Tompkins models.

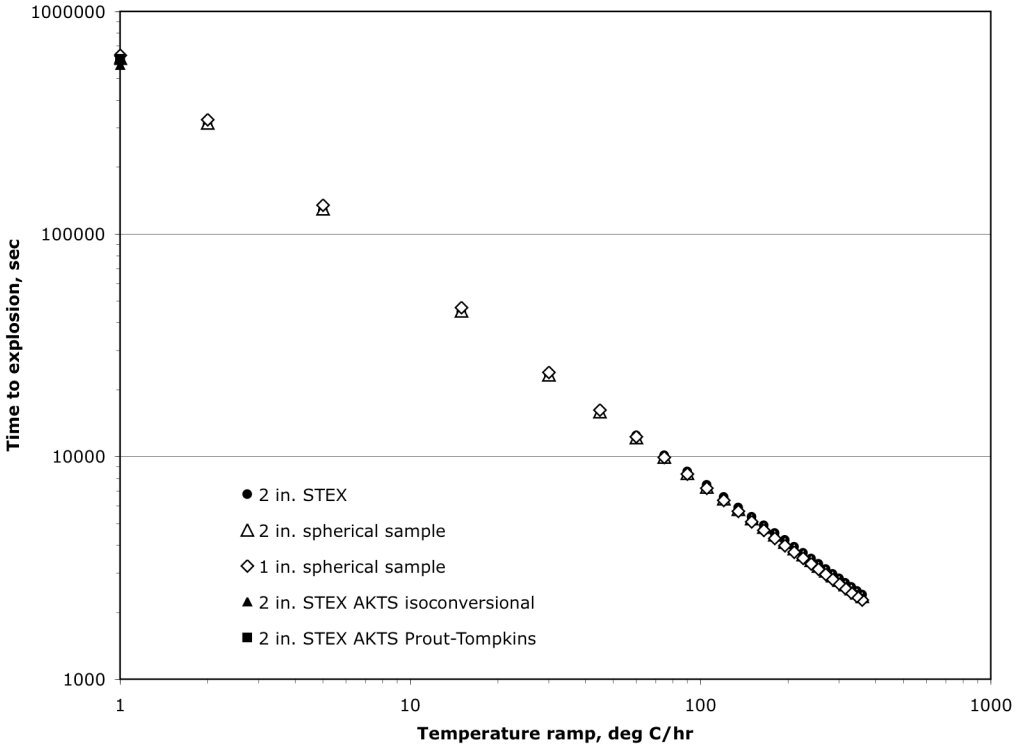

Figure 12a. Ramped simulation time to explosion.

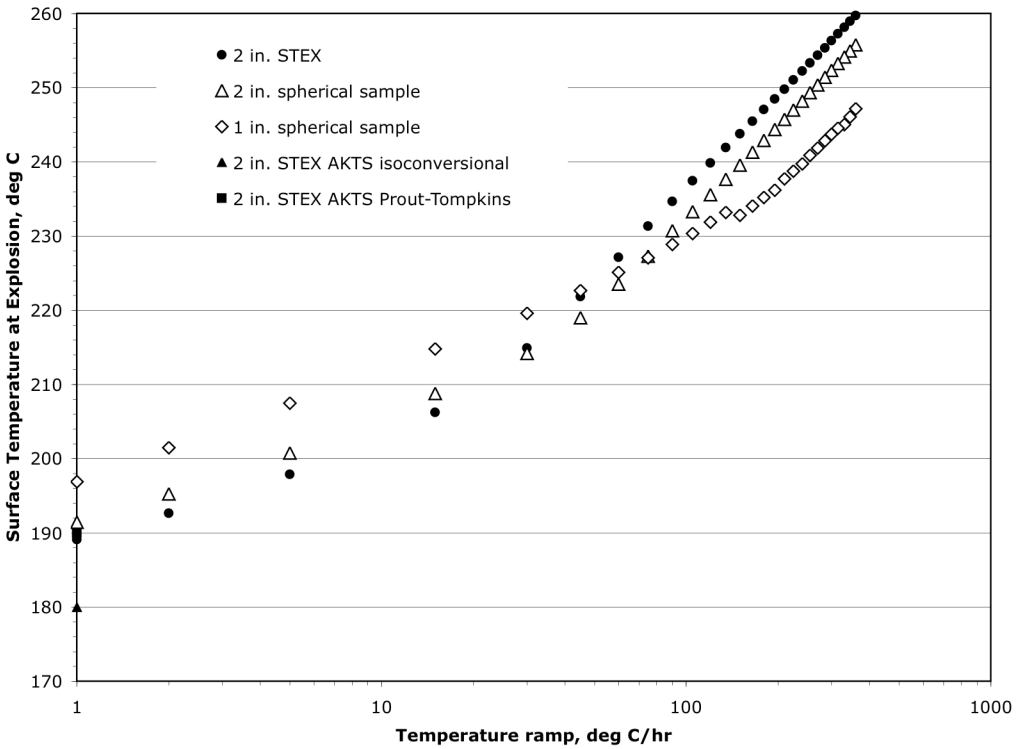

Figure 12b. Ramped simulation surface temperature at explosion

Effects of beta-delta phase transition kinetics on STEX simulations

The two-reaction bidirectional autocatalytic model previously described was also used for the beta-delta transition in the STEX simulations. Figures 13a shows that the particular kinetics model used has little effect on the time to explosion. However, Figure 13b shows that the two-reaction model using 165°C XRD parameters tend to predict lower surface temperatures at explosion than the other two models, especially at ramp rates above 10°C/hr. Further investigation into these simulations show that the β-HMX decomposition is dominant in the two-reaction model using 165°C XRD parameters, while the δ-HMX decomposition is dominant in the other two kinetics models. This result, coupled with the findings from the ODTX simulation results, suggests that the faster time to explosion may be due to the fewer reaction steps required for the direct $\beta \rightarrow p$ transition compared to the $\beta \rightarrow \delta \rightarrow p$ transition. More detailed comparisons with STEX data are needed to determine which model is more correct.

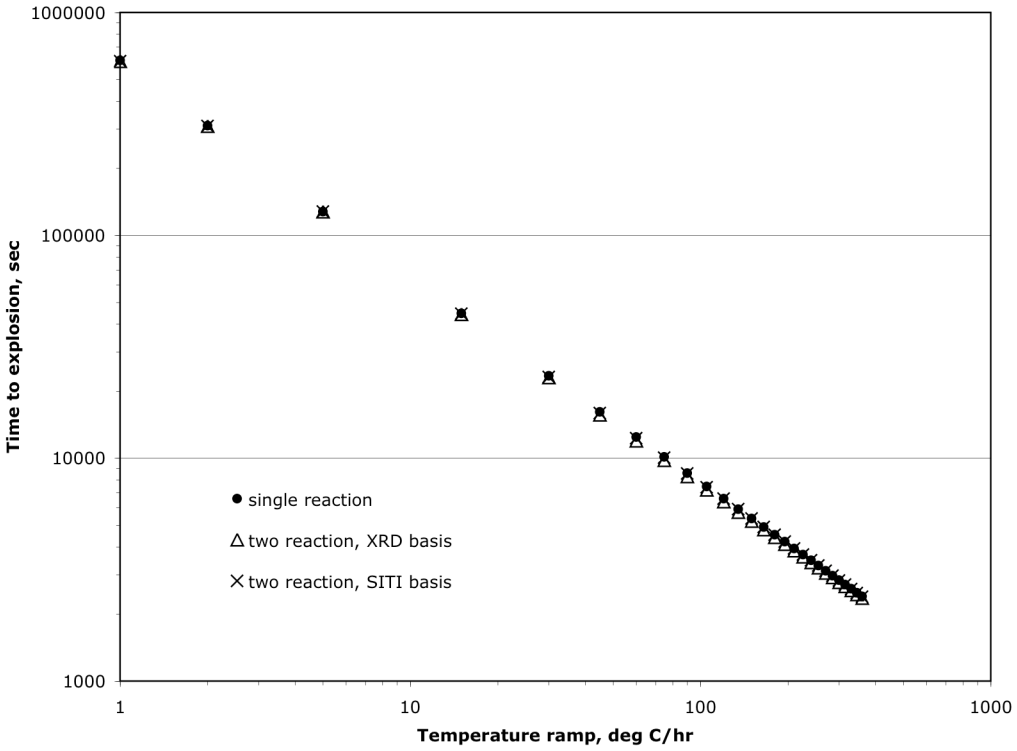

Figure 13a. Effect of beta-delta transition kinetics on the ramped simulation time to explosion.

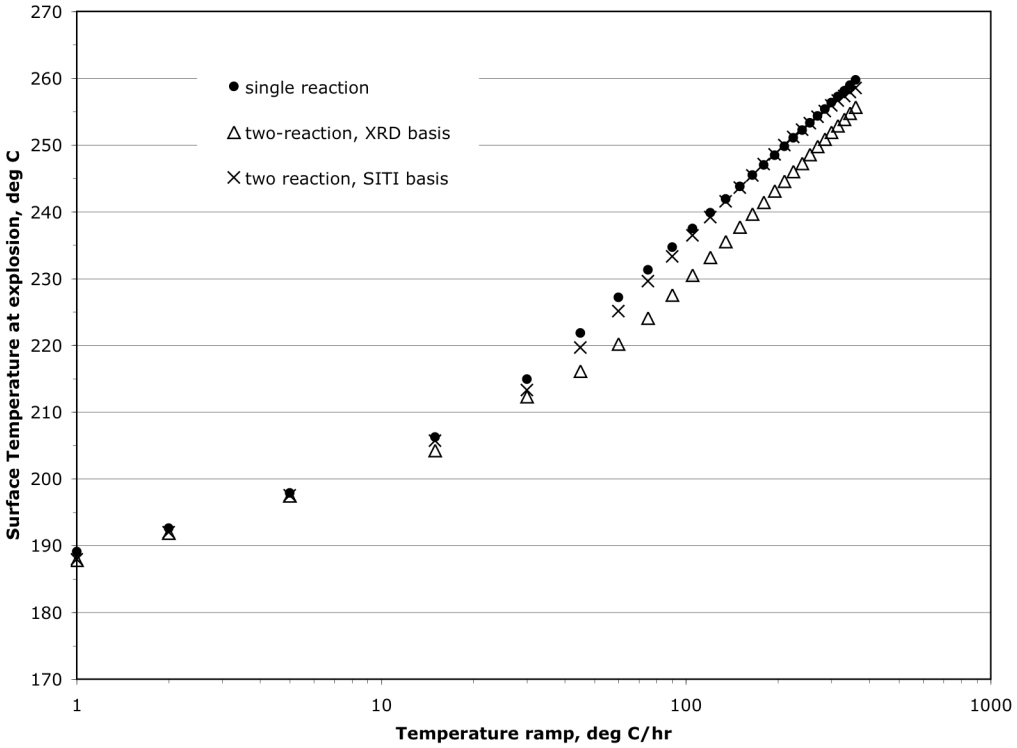

Figure 13b. Effect of beta-delta transition kinetics on the ramped simulation surface temperature at explosion.

Conclusions

The preliminary results shown here suggest that the chemical kinetics models in ALE3D provide sufficient mechanics to model both ODTX and STEX experiments of HMX. The data collected from using the ALE3D tend to be in good agreement with simulations of the AKTS Thermal Safety program, and the characteristic trends exhibited by the ALE3D data are similar to those encountered in experiments. However, more work needs to be done in exploring the chemical kinetics encountered in various HMX phase transitions. In particular, the times to explosion for ODTX and STEX simulations are heavily dependent upon the beta-delta phase transition model for certain ranges of surface temperature or ramp rate. Nevertheless, the models shown here provide a sound basis for ODTX and STEX modeling. Therefore, these techniques may be extended for use with other types of high explosives.

Acknowledgements

The authors would like to thank Jack Yoh (LLNL) for his work in setting up the HMX materials model in ALE3D, Rich Becker (LLNL-NTED) for providing information regarding the setup of a two-dimensional simulation in ALE3D, and Al Nichols (LLNL-CCHED) for the implementation of ALE3D's pseudospecies capability.

References

Burnham A. K. (2000) Application of the Sestak-Berggren equation to organic and inorganic materials of practical interest, *J. Therm. Anal.& Cal.* **60**, 895-908.

Burnham A. K. and Braun R. L. (1999), Global kinetic analysis of complex materials, *Energy & Fuels* **13**, 1-22.

Burnham A. K., Weese R. K., and Weeks B. L. (2004) A distributed activation energy model of thermodynamically inhibited nucleation and growth reactions and its application to the β–δ phase transition of HMX, *J. Phys. Chem*. **108**, 19432-19441.

Erikson W. W. (2005) Application of Global Decomposition Models to Energetic Material Cookoff, Presented at JANNAF 40th CS, 28th APS, 22nd PSHS, and 4th MSS Joint Meeting, Charleston, SC, June 2005.

Friedman H. L. (1964) Kinetics of thermal degradation of char-forming plastics from thermogravimetry. Application to a phenolic plastic, *J. Polymer Sci.* **C6**, 183-195.

Incropera F. P. and DeWitt D. P., *Fundamentals of Heat and Mass Transfer*, 4th ed. (Wiley, New York, 1996).

Kaneshige M. J., Renlund A. M., Schmitt R. G., Erikson W. W. (2002) Cook-off experiments for model validation at Sandia National Laboratory, *12th Intl. Det. Symp*., San Diego, ONR 333-05-2, pp. 821-830.

Ozisik M. N., *Heat Conduction* (Wiley, New York, 1980).

Roduit B., Borgeat C., Ticmanis U., Kaiser M., Guillaume P., Berger B., and Folly P. (2004) Thermal stability and safety analysis of explosives under different temperature modes, *35th International Annual Conference of ICT*, 37-1.

Wemhoff A. P. and Burnham A. K. (2006), Calibration of Parameters in Beta-Delta Phase Transformation Kinetics Using Computer Simulations, *Lawrence Livermore National Laboratory*, Report UCRL-TR-218130.

Yoh J. J., McClelland M. A., Maienschein J. L., Wardell J. F., and Tarver C. M. (2005) Simulating thermal explosion of cyclotrimethylenetrinitramine-based explosives: Model comparison with experiment, *J. Appl. Phys.* **97**, 083504.

Zaug J. M., Farber D. L., Saw C. K., and Weeks B. L. (2003) Kinetics of solid phase reactions at high temperature, *Lawrence Livermore National Laboratory*, Report UCRL-ID-147389 and supplemental viewgraphs.